Journal of Materials Science: Materials in Electronics (2019) 30:120–129
https://doi.org/10.1007/s10854-018-0274-8

# Excellent-$\Delta\varepsilon'$, very low-tanδ, giant-$\varepsilon'$ and nonlinear *J–E* properties of $Zn^{2+}$-doped $CaCu_3Ti_{4.1@4.2}O_{12}$ ceramics

**Chatchawal Sripakdee[1] · Krissana Prompa[2] · Kittipong Sitthikul[3] · Thanin Putjuso[3]**

Received: 11 September 2018 / Accepted: 22 October 2018 / Published online: 1 November 2018


**Abstract**
In this work, the dielectric properties of $Zn^{2+}$ doped $CaCu_3Ti_{4.1@4.2}O_{12}$ ($0 \le x \le 0.1$) ceramics were investigated. A giant dielectric constant ($\varepsilon' \sim 8955$–$20639$) and very low loss tangent ($\tan\delta \sim 0.005$–$0.015$) with an excellent temperature coefficient ($\Delta\varepsilon'$ less than $\pm 15\%$ over a temperature range of $\sim -60$–$180$ °C) were achieved in $CaCu_{2.90}Zn_{0.10}Ti_{4.1}O_{12}$ and $CaCu_{2.95}Zn_{0.05}Ti_{4.2}O_{12}$ ceramics sintered at 1080 °C and 1100 °C for 8 h. The very low tanδ and excellent $\Delta\varepsilon'$ obtained in these ceramics was due to a very high grain boundary resistance ($R_{gb}$), caused by the high density of grains and the presence of a $TiO_2$-rich phase at the GBs. These excellent dielectric properties suggest a potential application for use in high temperature X7R and X8R capacitors. It was found that the tanδ values decreased with increasing sintering temperature due to an increase in a $TiO_2$-rich phase. Nonlinear characteristics were observed in all ceramics, with significant enhancements in the nonlinear coefficient ($\alpha$) and breakdown field ($E_b$) due to $Zn^{2+}$doping. The best dielectric properties, $\varepsilon'$ (17598), tanδ (0.005), $\alpha$ (13.10) and $E_b$ (5401.70 V·cm$^{-1}$), with excellent-$\Delta\varepsilon'$ (−60–190 °C), were achieved in a $CaCu_{2.95}Zn_{0.05}Ti_{4.2}O_{12}$ ceramic sintered at 1100 °C for 8 h.

## 1 Introduction

Recently very high-performance dielectrics were developed with a giant dielectric constant (giant-$\varepsilon'$), very low loss tangent ($\tan\delta < 0.05$) and with excellent dielectric constant temperature stability ($\Delta\varepsilon' < \pm 15\%$ over a wide range of temperature). They also exhibited a very good nonlinear *J–E* characteristic in $CaCu_3Ti_4O_{12}$ (CCTO)-based materials [1–12] and other compounds [13–23]. Such materials can be useful in applications for capacitors, varistors and memory devices. Capacitors can store electrical energy while connected to a charging circuit, whereas varistors can provide over-voltage protection. Many approaches have been suggested to improve the properties of these ceramics to enhance their electrical and nonohmic properties for commercial applications. These include doping and preparation with CCTO [24–27], doping with CCTO/CTO [28–30], co-doping with CCTO [2, 31, 32] and doping with CCTO/$TiO_2$ [33, 34]. Although many researchers have studied their electrical properties, the simultaneous attainment of CCTO-based ceramics with suitable properties (i.e., giant-$\varepsilon'$, low-tanδ and high nonlinear properties) has rarely been reported [35–37], especially for $TiO_2$-rich $CaCu_3Ti_4O_{12}$ ceramics. Recently, we successfully achieved very high-performance dielectrics (giant-$\varepsilon' \sim 9200$ and low $\tan\delta \sim 0.017$) with an excellent $\Delta\varepsilon' < \pm 15\%$ in the temperature range of −55 to 210 °C in a ceramic with a nominal composition of $CaCu_{2.95}Zn_{0.05}Ti_{4.1}O_{12}$ [33]. Furthermore, very good dielectric properties ($\varepsilon' \sim 14012$ and $\tan\delta \sim 0.009$) and excellent-$\Delta\varepsilon' < \pm 15\%$ in the temperature range of −55 to 210 °C were achieved in a $CaCu_{2.9}Mg_{0.10}Ti_{4.2}O_{12}$ ceramic

✉ Thanin Putjuso
thanin.put@rmutr.ac.th

Chatchawal Sripakdee
chatchawal.s@rmutp.ac.th

Krissana Prompa
krissana@kkumail.com

Kittipong Sitthikul
ksitthikul@gmail.com

[1] Department of Science, Faculty of Science and Technology, Rajamangala University of Technology Phra Nakhon, Bangkok 10800, Thailand

[2] Integrated Nanotechnology Research Center (INRC), Department of Physics, Faculty of Science, Khon Kaen University, Khon Kaen 40002, Thailand

[3] School of General Science, Faculty of Liberal Arts, Rajamangala University of Technology Rattanakosin, Wang Klai Kangwon Campus, Hua Hin 77110, Prachaub Khiri Khan, Thailand

[34]. It has been suggested that these ceramics are suitable for application in high temperature X9R capacitors. In order to more extensively investigate the electrical and nonlinear *J–E* curve properties of $TiO_2$-rich $CaCu_3Ti_4O_{12}$ ceramics, $Zn^{2+}$-doped $CaCu_3Ti_{4.1}O_{12}$ and $CaCu_3Ti_{4.2}O_{12}$ ($Zn^{2+}$-doped $CaCu_3Ti_{4.1@4.2}O_{12}$) ceramics were considered. In this work, $Zn^{2+}$-doped $CaCu_3Ti_{4.1@4.2}O_{12}$ ceramics ($0 \le x \le 0.1$) were obtained using a polymer pyrolysis (PP) chemical route [33, 38]. $Zn^{2+}$ doping effects on the dielectric properties ($\varepsilon'$ and tanδ), $\Delta\varepsilon'$ and nonlinear *J–E* properties of these ceramics were investigated. Surprisingly, a giant-$\varepsilon' \sim 8955$–$20639$ with a very low $\tan\delta \sim 0.005$–$0.015$ and excellent $\Delta\varepsilon' < \pm 15\%$ over a temperature range of $\sim -60$–$180\,^{\circ}C$ were obtained in $CaCu_{2.90}Zn_{0.10}Ti_{4.1}O_{12}$ and $CaCu_{2.95}Zn_{0.05}Ti_{4.2}O_{12}$ ceramics sintered at 1080 °C and 1100 °C for 8 h. The excellent properties of these ceramic samples likely resulted from

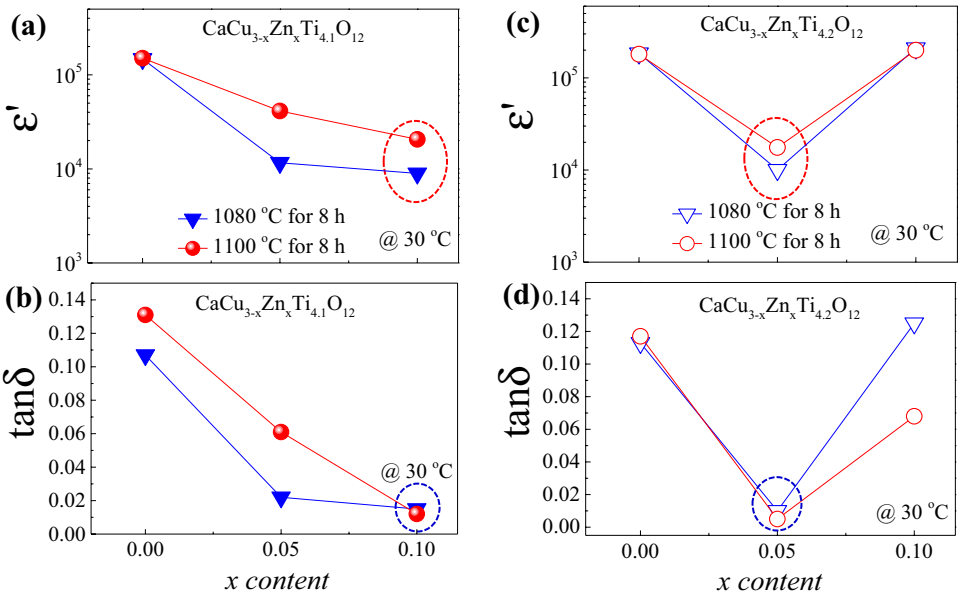


**Fig. 1** **a–d** Display $\varepsilon'$ and tanδ values at 30 °C and 1 kHz of $CaCu_{3-x}Zn_xTi_{4.1}O_{12}$ and $CaCu_{3-x}Zn_xTi_{4.2}O_{12}$ ($x = 0.00$–$0.10$) ceramics sintered under various conditions

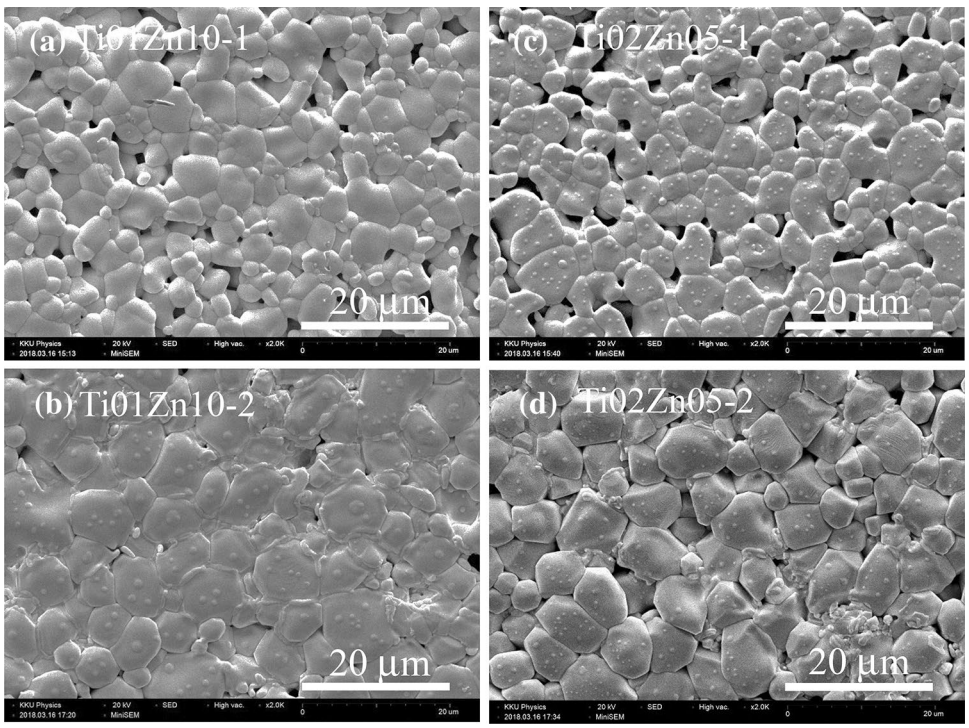


**Fig. 2** SEM images of polished surface morphology of **a** Ti1Zn10-1, **b** Ti1Zn10-2, **c** Ti2Zn05-1 and **d** Ti2Zn05-2 ceramics

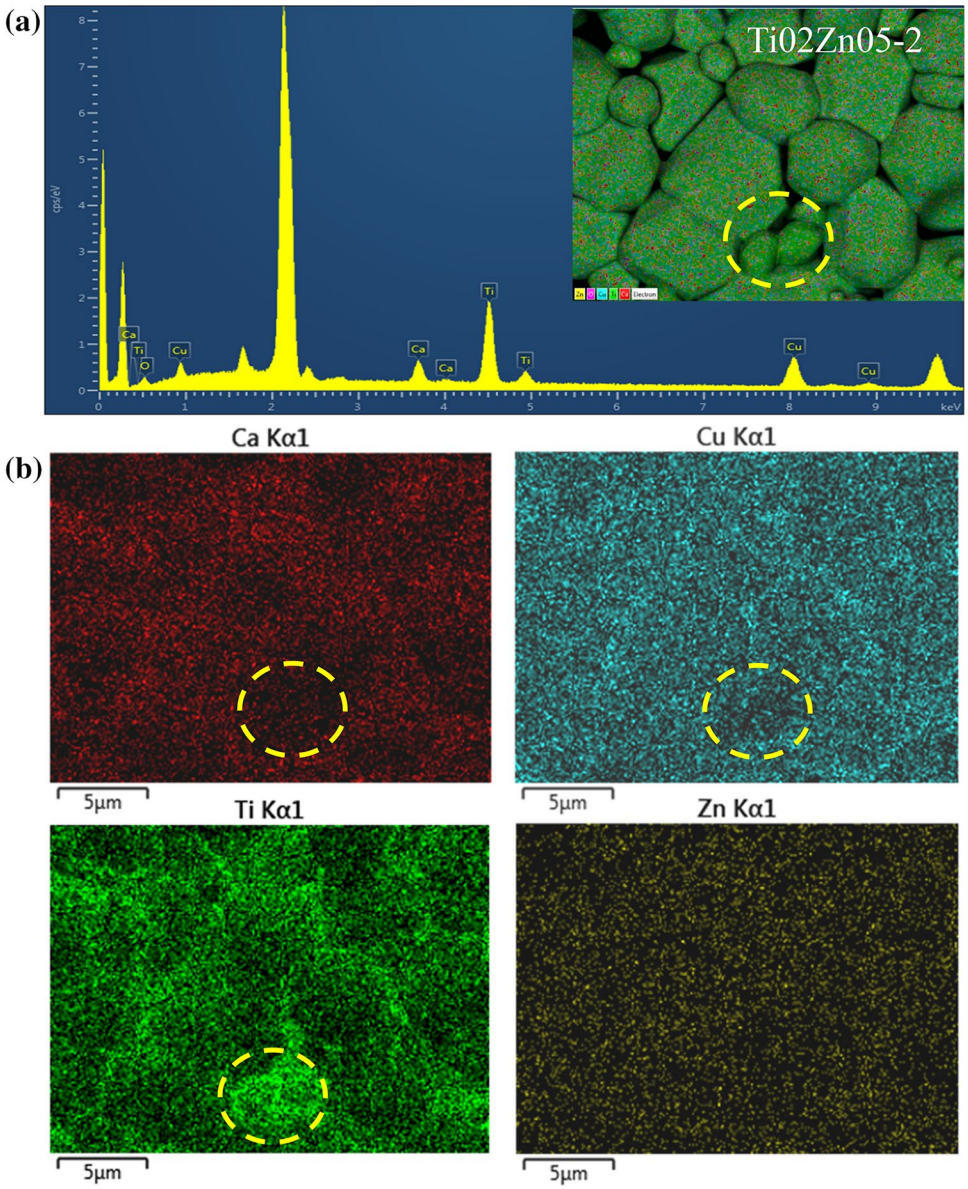


**Fig. 3** **a** EDXS spectra of the Ti02Zn05-2 ceramics; inset displays the SEM mapping images for a mixture of all elements, **b** elemental mapping of the Ti02Zn05-2 ceramics for Ca, Cu, Ti and Zn

the development of oxygen vacancies at grain boundaries ($O_{GB}$). In addition to the dielectric properties, nonlinear *J–E* characteristics of these ceramics were measured and found to have α and $E_b$ values of approximately 49.66 and 13146.25 $V \cdot cm^{-1}$, respectively.

## 2 Experimental details

$Zn^{2+}$-doped $CaCu_3Ti_{4.1@4.2}O_{12}$ ceramics with a nominal composition of $CaCu_{3x}Zn_xTi_{4.1}O_{12}$ and $CaCu_{3-x}Zn_xTi_{4.2}O_{12}$ (x = 0.00–0.10) were synthesized by a PP process [27, 34, 38]. $CH_2$=CHCOOH, $(NH_4)_2S_2O_4$, $Cu(NO_3)_2 \cdot 3H_2O$, $Ca(NO_3)_2 \cdot 4H_2O$, $Zn(NO_3)_2 \cdot 6H_2O$ and $C_{16}H_{28}O_6Ti$ were used as the starting materials. The process of calcining powders and ceramic samples with these compositions has been described elsewhere [33, 38]. All $Zn^{2+}$-doped $CaCu_3Ti_{4.1@4.2}O_{12}$ ceramics were obtained by sintering pellet samples in air under sintering conditions of 1080 °C or 1100 °C for 8 h.

The polished surface microstructure and energy-dispersive X-ray spectrometry (EDXS) mapping of the ceramics were investigated using field emission scanning electron microscopy (FESEM; JSM-6510LV JEOL). Average grain sizes (AGs) of ceramics were calculated using the standard line intercept technique. The X-ray diffraction profile of all ceramics were characterized by X-ray Diffractometry (XRD) (Bruker BioSpin AG; Bruker/D8 Advance). The crystal structure of the ceramics was compared with the crystallographic structure of the CCTO and $TiO_2$ standards

using X′ Pert High Score Plus software. Capacitance (C) and dielectric loss tangents (tanδ) of all ceramics were measured at various frequencies ($10^2$–$10^6$ Hz) and temperatures (−60 to 220 °C) using an impedance gain phase analyzer (Hewlett Packard 4194A). The dielectric constants ($\varepsilon'$) were calculated using Eq. (1) in our previous report [27]. The *J–E* curves of all ceramics were characterized using a high voltage measurement unit (Keithley Model 247). Significant parameters of the nonlinear *J–E* characteristic (nonlinear coefficient, $\alpha$ and breakdown electric field, $E_b$) of all ceramics were obtained as described elsewhere [33]. To confirm the presence of $Ti^{3+}$ in the ceramics, the $Ti^{3+}/Ti^{4+}$ ratio [38] of the Ti oxidation state was measured using an X-ray absorption near edge structure (XANES) technique employing multiple X-ray techniques (electron energy of $4\times10^3$–$18\times10^3$ eV; $10^7$–$10^{10}$ photon $s^{-1}$; beam current $10^{-1}$ A). Ti K-edge XANES spectra were obtained in an energy range of 4940–5040 eV using an energy step of 0.2 eV. The normalized XANES data were analyzed using the ATHENA software that is part of an IFEFFIT package [39, 40].

## 3 Results and discussion

In general, giant-$\varepsilon'$ values are quite consistent with very high tanδ values in CCTO-based compounds [41, 42]. Therefore, optimization of very high-performance dielectric properties (giant-$\varepsilon'$ with low-tanδ) of $CaCu_{3-x}Zn_xTi_{4.1}O_{12}$ and $CaCu_{3-x}Zn_xTi_{4.1}O_{12}$ ceramics should be considered. As illustrated in Fig. 1, although $\varepsilon'$ and tanδ values of $CaCu_{3-x}Zn_xTi_{4.1}O_{12}$ and $CaCu_{3-x}Zn_xTi_{4.2}O_{12}$ ceramics changed remarkably, irrespective of the *x* value or sintering conditions, the $\varepsilon'$ values of these ceramics are still too high (greater than 8000). As seen in Fig. 1a, b, increased $Zn^{2+}$ doping of the $CaCu_{3-x}Zn_xTi_{4.1}O_{12}$ ceramics gives rise to decreases in both $\varepsilon'$ and tanδ values. At 1 kHz and RT, very low-tanδ (less than 0.016) with giant-$\varepsilon'$ (higher than 8000) values were achieved in the $CaCu_{2.95}Zn_{0.05}Ti_{4.1}O_{12}$ (x = 0.05) ceramic sintered at 1080 °C for 8 h and $CaCu_{2.90}Zn_{0.10}Ti_{4.1}O_{12}$ (x = 0.10) ceramic sintered at 1080 °C and 1100 °C for 8 h. However, the undoped $CaCu_3Ti_{4.1}O_{12}$ (x = 0.00) sintered at 1080 °C and 1100 °C for 8 h, and $CaCu_{2.95}Zn_{0.05}Ti_{4.1}O_{12}$ (x = 0.05) ceramics sintered at 1100 °C for 8 h displayed tanδ values higher than 0.05 (tanδ > 0.05), which is unacceptable for capacitor applications. Interestingly, the tanδ values of the $CaCu_{2.90}Zn_{0.10}Ti_{4.1}O_{12}$ (x = 0.10) ceramic significantly decreased with increasing sintering temperature, whereas their $\varepsilon'$ values increased. Generally, both $\varepsilon'$ and tanδ values increase with increasing sintering temperature [43, 44].

As shown in Fig. 1c, d, very low-tanδ and giant-$\varepsilon'$ values were achieved only for the $CaCu_{2.95}Zn_{0.05}Ti_{4.2}O_{12}$ (x = 0.05) ceramics sintered at 1080 °C and 1100 °C for 8 h, while the other ceramics (with x = 0.00 and x = 0.10) are not useable for capacitor applications (tanδ > 0.05). It is interesting

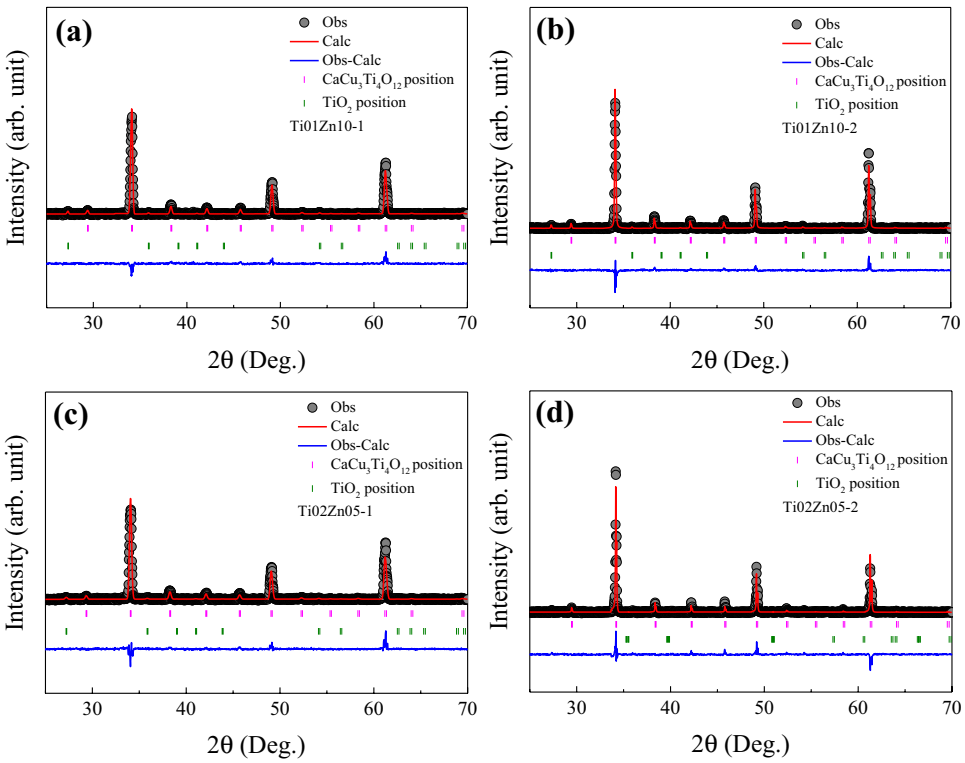


**Fig. 4** Rietveld refinement profiles fitted for **a** Ti01Zn10-1, **b** Ti01Zn10-2, **c** Ti02Zn05-1 and **d** Ti02Zn05-2 ceramics

that the very low tanδ ~ 0.005 and giant-$\varepsilon'$ ~ 17598 values obtained in $CaCu_{2.95}Zn_{0.05}Ti_{4.2}O_{12}$ (x = 0.05) ceramics sintered at 1100 °C for 8 h have never before been observed in CCTO-based ceramics [24, 25, 31–33, 35, 37] and other $TiO_2$-based ceramics [14, 45–47]. This very low-tanδ (~ 0.005) obtained in $CaCu_{2.95}Zn_{0.05}Ti_{4.2}O_{12}$ ceramic is about ~ 3.4 times lower than that of the $CaCu_{2.95}Zn_{0.05}Ti_{4.1}O_{12}$ ceramic (tanδ ~ 0.017) in our work [33]. Notably, the very high performance dielectric properties obtained in $CaCu_{2.95}Zn_{0.05}Ti_{4.2}O_{12}$ ceramic can be increased more than in another ceramic compounds [13, 15, 16, 48–50].

From Fig. 1, very low-tanδ and giant-$\varepsilon'$ were observed in the $CaCu_{2.90}Zn_{0.10}Ti_{4.1}O_{12}$ (x = 0.10) ceramics sintered at 1080 °C and 1100 °C for 8 h (denoted as Ti01Zn10-1 and Ti01Zn10-2, respectively), and the $CaCu_{2.95}Zn_{0.05}Ti_{4.2}O_{12}$ ceramics sintered at 1080 °C and 1100 °C for 8 h (denoted as Ti02Zn05-1 and Ti02Zn05-2, respectively). Therefore, these four ceramics were used to further investigate the underlying mechanisms of the origin of this significantly enhanced dielectric response.

Figure 2a–d shows SEM images of the polished surfaces of Ti01Zn10-1, Ti01Zn10-2, Ti02Zn05-1 and Ti02Zn05-2 ceramics, respectively. The AGs of Ti01Zn10-1, Ti01Zn10-2, Ti02Zn05-1 and Ti02Zn05-2 ceramics were found to be 3.87 ± 0.02, 5.17 ± 0.05, 3.14 ± 0.02 and 4.56 ± 0.02 μm, respectively. The grain sizes of each ceramic were quite similar and increased slightly with increasing sintering temperature. Notably, the AGs of Ti01Zn10-2 and Ti02Zn05-2 ceramics were about ~ 1.33 and ~ 1.45 times higher than those of the Ti01Zn10-1 and Ti02Zn05-1 ceramics, respectively. The AGs of these four ceramics are smaller than those of the $Zn^{2+}$ doped CCTO-based ceramics [33, 51].

The distribution of major (Ca, Cu, Ti, and O) and doping (Zn) elements in all ceramics were examined using elemental mapping combined with an EDXS technique. As illustrated in Fig. 3a, the EDXS results of the areas displayed in the inset for the Ti02Zn05-2 ceramic confirms the presence of Ca, Cu, Ti and O, whereas the Zn was not detected. This was due to the similarly of the energy values of the X-ray emissions of $Zn^{2+}$ (~ 1.011 keV) and $Cu^{2+}$ (~ 0.929 keV), which is similar to previous reports of $Zn^{2+}$ doped CCTO-based compound [51]. Additionally, EDXS results for the other selected ceramics were also measured (data not shown). As displayed in the inset of Fig. 3a, the image confirms the presence of Ca, Cu, Ti, and Zn (Fig. 3b). As seen in Fig. 3b, the $TiO_2$-rich phase (yellow dashed circles) was observed in the small grain regions as well as along grain boundaries in Ti02Zn05-2 ceramics. Additionally, only Ti and O (data not shown) elemental mapping were detected in the yellow dashed circles. It was also found that the $TiO_2$-rich phase increased with increasing sintering temperature and/or increasing Ti content.

Figure 4a–d display the Rietveld refinement profile fits for the XRD patterns of Ti01Zn10-1, Ti01Zn10-2, Ti02Zn05-1 and Ti02Zn05-2 ceramics, respectively. The Rietveld refinement details for the analysis of $R$ ($R_{exp}$, $R_{wp}$, and $R_p$) values and goodness of fit (*GOF*) have been reported [38, 52]. *GOF* values of these ceramics occurred in a narrow range

**Table 1** Lattice parameter ($a$) and structural data obtained from the Rietveld refinement of all ceramic samples

| Samples | $a$ (Å) | $R_{exp}$ (%) | $R_p$ (%) | $R_{wp}$ (%) | GOF |
|---|---|---|---|---|---|
| Ti01Zn10-1 | 7.393(0) | 3.853 | 4.865 | 6.203 | 2.590 |
| Ti01Zn10-2 | 7.392(1) | 3.853 | 4.407 | 5.553 | 2.076 |
| Ti02Zn05-1 | 7.391(3) | 3.770 | 4.377 | 5.466 | 2.102 |
| Ti02Zn05-2 | 7.391(3) | 3.770 | 4.377 | 5.466 | 2.102 |

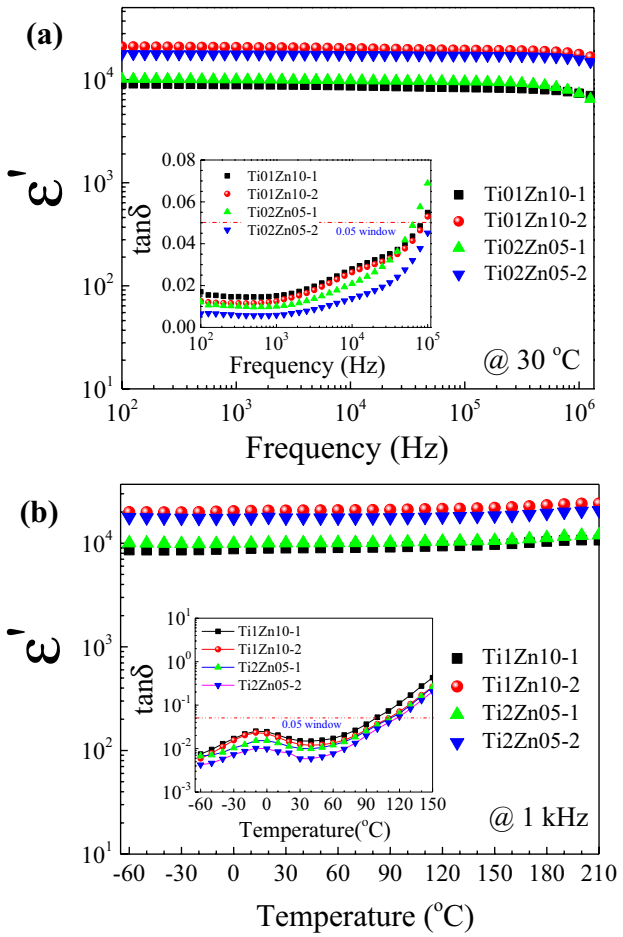


**Fig. 5** **a, b** Display frequency ($10^2$–$10^6$ Hz) and temperature (− 65 to 210 °C) dependence of $\varepsilon'$ for Ti01Zn10-1, Ti01Zn10-2, Ti02Zn05-1 and Ti02Zn05-2 ceramics; their insets show tanδ values as a function of frequency ($10^2$–$10^5$ Hz) and temperature (− 65 to 150 °C), respectively

of ~ 2.0−2.5. The percentages of *R* factors for these ceramics are in the appropriate range of approximately 3−6%. Lattice parameters (*a*) of these ceramics were comparable with those of the CCTO standard ($a = 7.391$ Å) [53]. They were found to be 7.393(0), 7.392(1), 7.391(3), 7.391(3) Å for Ti01Zn10-1, Ti01Zn10-2, Ti02Zn05-1 and Ti02Zn05-2 ceramics, respectively. It is clear that the *a* value shows no significant variation under the sintering temperatures examined in the current study. However, the *a* value decreased slightly with increasing $Zn^{2+}$ dopant content. This suggests that substitution of $Zn^{2+}$ (0.74 Å) into $Cu^{2+}$ (0.73 Å) sites has an important role in the stability of this CCTO cubic structure. As illustrated in Fig. 4a–d, the profile fits for the main peaks of ceramics correspond to those of the $CaCu_3Ti_4O_{12}$ (ICSD card No. 95714) and $TiO_2$ (ICSD card No. 26715) standards. This confirmed the presence of the $CaCu_3Ti_4O_{12}$ and $TiO_2$ phases in all ceramic samples. From the Rietveld refinement fitting profiles, the $CaCu_3Ti_4O_{12}$:$TiO_2$ ratios of Ti1Zn10-1, Ti1Zn10-2, Ti2Zn05-1 and Ti2Zn05-2 ceramics were found to be 96.3:3.7, 95.9:4.1, 96.5:3.5 and 99.9:0.1, respectively. In addition to a minor $TiO_2$ phase, no other impurity phases (i.e., CuO, $Cu_2O$ and related-oxide Zn phase) were observed. This confirms a complete substitution of $Zn^{2+}$ ions into the $CaCu_{3x}Zn_xTi_{4.1}O_{12}$ and $CaCu_{3-x}Zn_xTi_{4.2}O_{12}$ ceramics. The relative densities of these ceramics were greater than 93%, comparable to the standard values [53] (Table 1).

Figure 5a and its inset display $\varepsilon'$ and tanδ values as a function of frequency for the Ti01Zn10-1, Ti01Zn10-2, Ti02Zn05-1 and Ti20Zn05-2 ceramics, respectively. As seen in this Figure, the $\varepsilon'$ values of all of these ceramics were slightly frequency dependent over a range of $10^2$–$10^6$ Hz, whereas tanδ values were smaller than 0.05 over the frequency range of ~ $10^2$–$8 \times 10^4$ Hz. At 1 kHz and 30 °C, the $\varepsilon'$ values of the Ti01Zn10-1, Ti01Zn10-2, Ti02Zn05-1 and Ti20Zn05-2 ceramics were found to be 8955, 20693, 10035 and 17598, while the tanδ values were 0.015, 0.012, 0.010 and 0.005, respectively. It is interesting that excellent dielectric properties (especially giant-$\varepsilon'$ ~ 17598 with a very low tanδ ~ 0.005) obtained in Ti02Zn05-2 ceramic have never been reported in other CCTO-based ceramics. Notably, the sintering temperature effects can reduce tanδ values about 1.25 and 2 times, whereas that of $\varepsilon'$ values increase about 2.3 and 1.76 times for Ti01Zn10 and Ti02Zn05 ceramics, respectively. These improvements in the $\varepsilon'$ and tanδ values may have been due to the increased grain boundary resistant ($R_{gb}$) caused by the effect of grain density [54, 55]. The giant-$\varepsilon'$ and low-tanδ values of all ceramics were comparable to those of other CCTO-based ceramics [25, 26, 34, 43, 44, 51, 56]. The $\varepsilon'$ and tanδ values as a function of temperature (− 60 to 210 °C) are shown in Fig. 5b and its inset, respectively. It can be seen that $\varepsilon'$ values of all ceramics are slightly dependent over the temperature range of − 60 to 210 °C, whereas tanδ values were less than 0.05 over the temperature range of − 60 to 90 °C for Ti01Zn10-1, and − 60 to 110 °C for other ceramics (Ti01Zn10-2, Ti02Zn05-1 and Ti20Zn05-2). It can be concluded that these ceramic samples display very good temperature stability for both tanδ and $\varepsilon'$.

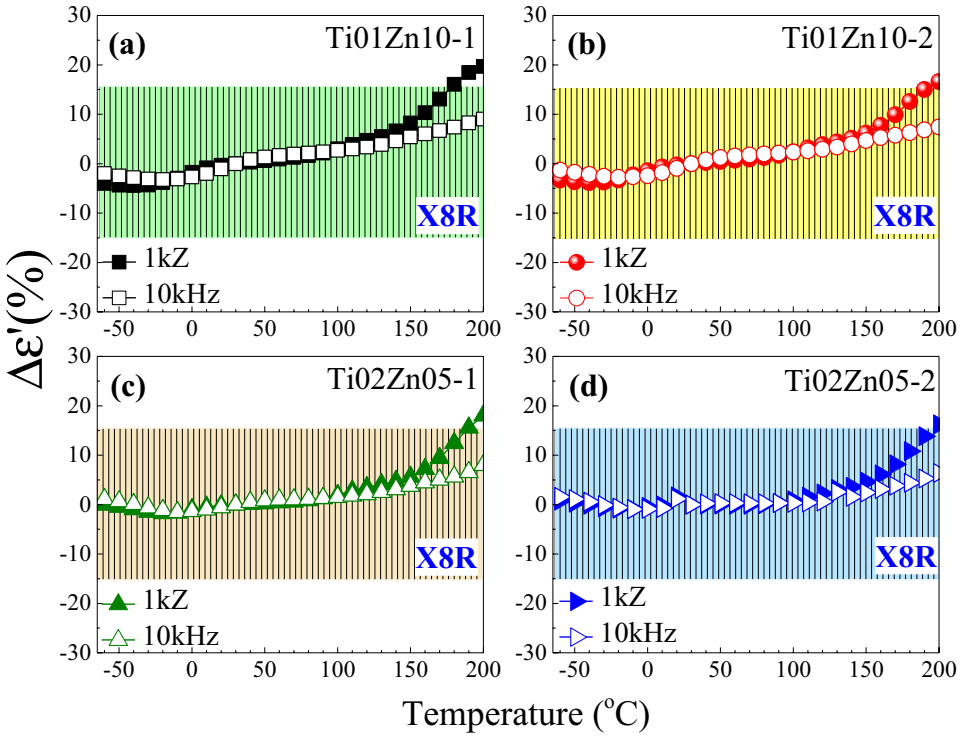


**Fig. 6** **a–d** Display temperature coefficients of dielectric constant ($\Delta\varepsilon'$) for ceramic samples sintered at 1060 °C for 8 h and 1100 °C for 5 h

**Table 2** Dielectric constant ($\varepsilon'$) and loss tangent (tanδ) at 30 °C and 1 kHz, temperature range for $\Delta\varepsilon'$ with values less than ± 15%, grain ($R_g$) and grain boundary ($R_{gb}$) resistance (at 150 °C) of all ceramic samples

| Sample | $\varepsilon'$ | tanδ | $E_g$ (eV) | $E_{gb}$ (eV) | $R_g$ (Ω·cm) | $R_{gb}$ ($10^3$ Ω·cm) | ΔT (°C) of $\Delta\varepsilon'$ | ΔT (°C) of tanδ | α | $E_b$ (V·cm$^{-1}$) | $\varphi_B$ (eV) | $Ti^{3+}/Ti^{4+}$ (%) |
|---|---|---|---|---|---|---|---|---|---|---|---|---|
| Ti01Zn10-1 | 8955 | 0.015 | 0.054 | 0.769 | 30.4 | 470.7 | − 60 to 170 | − 60 to 90 | 297.38 | 5754.91 | 1.0126 | 4.00 |
| Ti01Zn10-2 | 20639 | 0.012 | 0.046 | 0.647 | 19.5 | 345.1 | − 60 to 180 | − 60 to 110 | 11.84 | 4460.25 | 0.9800 | 4.70 |
| Ti02Zn05-1 | 10035 | 0.010 | 0.038 | 0.794 | 58.5 | 738.8 | − 60 to 180 | − 60 to 110 | 36.87 | 6424.85 | 0.9875 | 4.92 |
| Ti02Zn05-2 | 17598 | 0.005 | 0.049 | 0.768 | 21.2 | 554.6 | − 60 to 190 | − 60 to 110 | 13.10 | 5401.70 | 0.9738 | 2.36 |

The very good dielectric properties of these ceramic samples was better than seen in other giant dielectric ceramics that used co-doping with $TiO_2$ oxide [45, 57] and doping/co-doping of CCTO-based ceramics [24, 31, 51].

For practical applications of these ceramics in electronic devices, a temperature coefficient of the dielectric constant ($\Delta\varepsilon' = (\varepsilon'_T - \varepsilon'_{30\,°C})/\varepsilon'_{30\,°C}$) of less than ± 15% should be achieved in addition to a suitable giant-$\varepsilon'$ and very low tanδ. Principally, the temperature range (ΔT) of the $\Delta\varepsilon'$ conditions is defined as − 55 to 150 °C and − 55 to 125 °C for X8R and X7R capacitors, respectively [58]. As seen in Fig. 6a–d, a ΔT of less than ± 15% of $\Delta\varepsilon'$ condition for all ceramics was calculated at 1 kHz (closed symbol) and at 10 kHz (open symbol). As can be clearly seen in Fig. 6a–d and the data given in Table 2, these ceramics comply with the EIA code for X8R and X7R capacitors. Remarkably, the best $\Delta\varepsilon'$ conditions were observed in Ti02Zn05-2 ceramics. At 1 kHz, $\Delta\varepsilon'_{190\,°C}$ $[(\varepsilon'_{190\,°C} - \varepsilon'_{30\,°C})/\varepsilon'_{30\,°C}]$ was 13.82%, whereas the $\Delta\varepsilon'_{200\,°C}$ (at 10 kHz) was 6.38%. These two values are smaller than those of other giant dielectric compounds derived from doping/co-doping $TiO_2$-based oxides [14, 45, 59], CCTO-based compounds [51, 60] and CCTO/CTO-composites [28–30, 61].

To understand the electrical heterogeneity of grains ($R_g$) and grain boundaries ($R_{gb}$) in all ceramics, their impedance complex plane plots ($Z^*$) were investigated. Generally, $R_{gb}$ can be determined using the large-semicircular arc (at low frequency), while $R_g$ values were estimated from small-semicircular arcs (at high frequency) [27]. As shown in Fig. 7a and its inset, at 30 °C a nonzero intercept on the x-axis and the linear part of the large semicircular arcs were observed. This is confirmation that the electrical responses in the ceramics consist of the effects of grains and grain boundaries (GBs). $R_g$ of Ti01Zn10 and Ti02Zn05 ceramics significantly decreased with increasing sintering temperature. However, the linear part of the large semicircular arcs tended to increase with increasing sintering temperature. It is remarkable that the highest linear-slope of the large semicircular arcs of Ti02Zn05-2 ceramic correlates with the lowest tanδ of this ceramic. It is notable that the sintering temperature effects on the $R_g$ and $R_{gb}$ values were concurrent with the improvement of giant-$\varepsilon'$ and very low-tanδ values obtained in each ceramic. As shown in Fig. 7b and its inset, a large semicircular arc and nonzero intercept decrease with increasing temperature. This indicates a decrease in $R_{gb}$ and $R_g$ values, respectively. Figure 7c, d, respectively, show plots of $\sigma_{gb}$ versus 1000/$T$, and $\sigma_g$ versus 1000/$T$, following the relationship, $\ln \sigma_{gb,g} = -E_{gb,g}/k_B T + \ln \sigma_0$ [38, 54]. The conduction activation energy at grain boundaries ($E_{gb}$) and in grains ($E_g$) was calculated from the slopes of the $\sigma_{gb}$ versus 1000/$T$, and $\sigma_g$ versus 1000/$T$ plots, respectively. The $E_{gb}$ and $E_g$ values are listed in Table 2. As illustrated in Table 2, as sintering temperature increased from 1080 to 1100 °C both

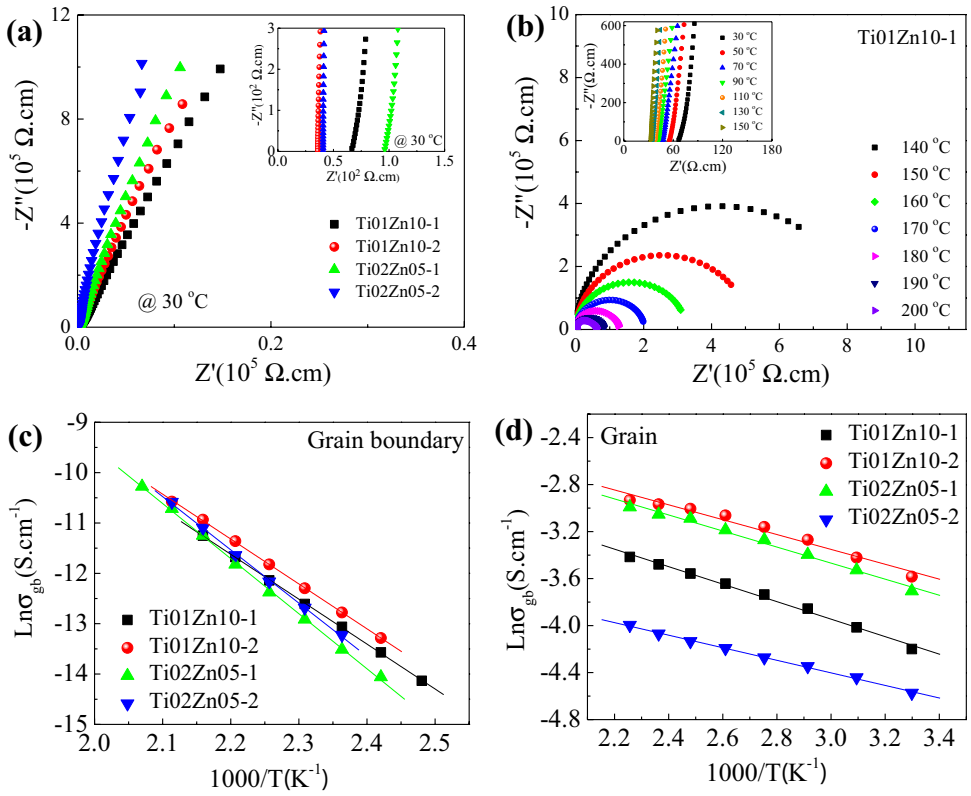


**Fig. 7** **a** And its inset display impedance complex plane plots ($Z^*$) at 30 °C and an expanded view of high frequency data close to the origin for all ceramics. **b** $Z^*$ plot and expanded view (inset) at various temperatures for Ti01Zn10-1. **c, d** Arrhenius plots of $\ln\sigma_{gb}$ and $\ln\sigma_g$ for all ceramics, respectively

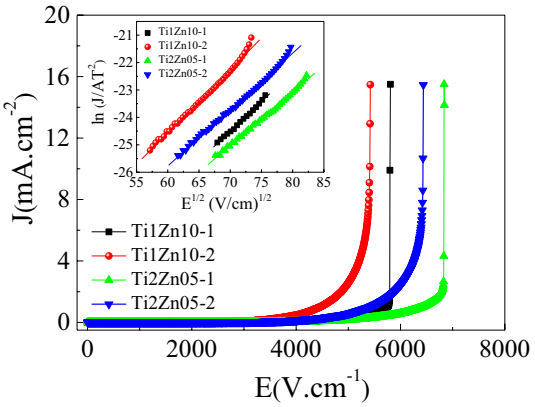


**Fig. 8** *J–E* curves at 30 °C for all ceramics; inset displays plots of ln ($J/AT^2$) versus $E^{1/2}$

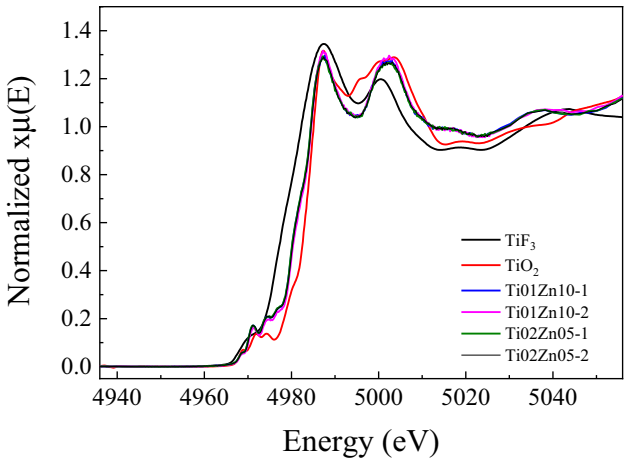


**Fig. 9** Normalized Ti XANES (K-edge) spectra of Ti01Zn10-1, Ti01Zn10-2, Ti02Zn05-1 and Ti02Zn05-2 ceramics compared with those of the $TiO_2$ and $TiF_3$ standards

the $E_{gb}$ and $E_g$ values of Ti01Zn10 and Ti02Zn05 ceramics decreased. This suggests that $E_g$ behavior is correlated with improvement of the giant-$\varepsilon'$ value, whereas $E_{gb}$ values were not correlated with tanδ values. As can be seen from the data listed in Table 2, the $E_{gb}$ values of Ti01Zn10-2 and Ti02Zn05-2 ceramics were approximately ~ 1.18 and ~ 1.03 times greater, while $E_g$ were about ~ 1.17 and ~ 1.28, lower than those of Ti01Zn10-1 and Ti02Zn05-1 ceramics, respectively.

Figure 8 displays the nonlinear *J-E* curves (at 30 °C) of all ceramics. In this Fig. 8, $\alpha$ and $E_b$ values were calculated and the data listed in Table 2. The $\alpha$ and $E_b$ values of Ti01Zn10 and Ti02Zn05 ceramics were inversely correlated with sintering temperature, caused by oxygen vacancies as the GBs increase. Notably, the $\varepsilon'$ values of Ti01Zn10-1 and Ti02Zn05-1 ceramics are about 2.32 and 1.75 times

lower than those values observed in the Ti1Zn10-2 and Ti2Zn05-2 ceramics, respectively. This behavior is similar to that observed in CCTO-based ceramics [32, 34, 54]. The reduction of $\alpha$ and $E_b$ values can result from a decrease in the $R_{gb}$ [62]. Furthermore, α values achieved in this work are comparable to those of other ceramics reported in the literature [2, 27, 38]. To gain a deeper understanding the electrical response at GBs, high potential barriers ($\varphi_B$) based on Schottky barriers were considered. Using the relationship, $\ln(J/AT^2) = (\beta E^{1/2} - \varphi_B)/k_B T$ [34, 63–67] and plotting $\ln(J/AT^2)$ versus $E^{1/2}$, the $\varphi_B$ and β values of all ceramics were found and are listed in Table 2. It is notable that $\varphi_B$ and $E_b$ values are inversely proportional, and decrease slightly with increasing sintering temperature. These $\varphi_B$ values (0.957–1.012 eV) are comparable with those reported in the literature [64, 65, 68].

Figure 9 displays the Ti XANES (K-edge) spectra of Ti01Zn10-1, Ti01Zn10-2, Ti02Zn05-1 and Ti02Zn05-2 ceramics, compared with those of the $TiO_2$ ($Ti^{4+}$) and $TiF_3$ ($Ti^{3+}$) standards. The edge energies of all ceramics were obtained using the XANES results, and the data are listed in Table 2. The edge energies of all the ceramics were nearer that of the $TiO_2$ than the $TiF_3$ standard. However, the presence of $Ti^{3+}$ was still detected, which was substantiated by a slight change in the Ti K-edge values of the XANES spectra. This is similar to that reported for other CCTO-based ceramics [38]. The $Ti^{3+}/Ti^{4+}$ (%) ratios of all ceramics were considered using Eq. (1) in our previous work [38], and the data are summarized in Table 2. It is found that both Ti01Zn10 and Ti02Zn05 ceramics display $Ti^{3+}/Ti^{4+}$ (%) ratios that increased with the sintering temperature. It is notable that the $Ti^{3+}/Ti^{4+}$ (%) ratios for Ti01Zn10-2 and Ti02Zn05-2 ceramics were higher than for Ti01Zn10-1 and Ti02Zn05-1 ceramics. Additionally, these results are consistent with the giant-$\varepsilon'$ observed in Ti01Zn10-2 and Ti02Zn05-2 ceramics. This may have resulted from an increase in oxygen vacancies inside the grains caused by the effects of sintering temperature. It can be concluded that there were *n*-type semiconducting grains in all ceramics, created from electron hopping between $Ti^{3+} \leftrightarrow Ti^{4+}$ sites in the structure. This may have been caused by an increase in oxygen vacancies resulting from sintering temperature and $TiO_2$.

## 4 Conclusions

Very good dielectric properties ($\varepsilon' \sim 8955$–$20639$, and $\tan\delta \sim 0.005$–$0.015$) with an excellent temperature coefficient ($\Delta\varepsilon' \leq \pm 15\%$) over a wide temperature range of $\sim -60$–$180$ °C were achieved in $CaCu_{2.90}Zn_{0.10}Ti_{4.1}O_{12}$ and $CaCu_{2.95}Zn_{0.05}Ti_{4.2}O_{12}$ ceramics sintered at 1080 °C and 1100 °C for 8 h. Moreover, the best $\Delta\varepsilon'$ condition [$\Delta\varepsilon'_{190\,^\circ C}$ $((\varepsilon'_{190\,^\circ C} - \varepsilon'_{30\,^\circ C})/\varepsilon'_{30\,^\circ C}) = 13.82\%$] was obtained in $CaCu_{2.95}Zn_{0.05}Ti_{4.2}O_{12}$ ceramics sintered at 1100 °C for 8 h. This is due to the high $R_{gb}$ values resulting from the presence of $TiO_2$ at the grain boundaries, substantiated by EDXS mapping. These ceramic samples are promising materials for EIA code X7R and X8R capacitors. The non-linear coefficients ($\alpha$) and breakdown fields ($E_b$) of the ceramics were enhanced by the doping/sintering effect. Very good α values (~ 11–297) and $E_b$ (~ 4460–6424 $V \cdot cm^{-1}$) were found in these ceramic samples. XANES results confirm the ratios of $Ti^{3+}/Ti^{4+}$ were enhanced in these ceramic samples.

**Acknowledgements** This work was financially supported by Rajamangala University of Technology Rattanakosin, Wang Klai Kangwon Campus, Hua Hin, Prachaubkerekhan, Thailand. It was also supported by the Thailand Research Fund through the Royal Golden Jubilee Ph.D. Program (PHD/0207/2558). We are also grateful to the Rajamangala University of Technology Phra Nakhon, Bangkok, Thailand, for their co-financial support. The Synchrotron Light Research Institute (SLRI), Nakhon Ratchasima, Thailand is acknowledged for XANES measurements.

## References

1. R. Schmidt, M.C. Stennett, N.C. Hyatt, J. Pokorny, J. Prado-Gonjal, M. Li, D.C. Sinclair, J. Eur. Ceram. Soc. **32**, 3313–3323 (2012)
2. J. Boonlakhorn, B. Putasaeng, P. Kidkhunthod, P. Thongbai, Mater. Des. **92**, 494–498 (2016)
3. J.-W. Lee, J.-H. Koh, Ceram. Int. **41**, 10442–10447 (2015)
4. T.B. Adams, D.C. Sinclair, A.R. West, Phys. Rev. B **73**, 094124 (2006)
5. J. Deng, X. Sun, S. Liu, L. Liu, T. Yan, L. Fang, B. Elouadi, Mater. Res. Bull. **88**, 320–329 (2017)
6. L. Liu, H. Fan, X. Chen, P. Fang, J. Alloy. Compd. **469**, 529–534 (2009)
7. L. Liu, H. Fan, P. Fang, L. Jin, Solid State Commun. **142**, 573–576 (2007)
8. L. Liu, H. Fan, L. Wang, X. Chen, P. Fang, Philos. Mag. **88**, 537–545 (2008)
9. L. Liu, H. Fan, P. Fang, X. Chen, Mater. Res. Bull. **43**, 1800–1807 (2008)
10. L. Liu, D. Shi, S. Zheng, Y. Huang, S. Wu, Y. Li, L. Fang, C. Hu, Mater. Chem. Phys. **139**, 844–850 (2013)
11. F. Han, S. Ren, J. Deng, T. Yan, X. Ma, B. Peng, L. Liu, J. Mater. Sci. Mater. Electron. **28**, 17378–17387 (2017)
12. Q. Zheng, H. Fan, J. Mater. Sci. Technol. **28**, 920–926 (2012)
13. J. Deng, L. Liu, X. Sun, S. Liu, T. Yan, L. Fang, B. Elouadi, Mater. Res. Bull. **88**, 320–329 (2017)
14. N. Thongyong, W. Tuichai, N. Chanlek, P. Thongbai, Ceram. Int. **43**, 15466–15471 (2017)
15. Z. Liu, H. Fan, S. Lei, X. Ren, C. Long, J. Eur. Ceram. Soc. **37**, 115–122 (2017)
16. X. Huang, W. Zhang, J. Xie, Q. Xu, L. Zhang, H. Hao, H. Liu, M. Cao, J. Mater. Sci. Mater. Electron. **28**, 4204–4210 (2017)
17. L. Yang, G. Huang, T. Wang, H. Hao, Y. Tian, Ceram. Int. **42**, 9935–9939 (2016)
18. Y. Huang, D. Shi, L. Liu, G. Li, S. Zheng, L. Fang, Appl. Phys. A **114**, 891–896 (2014)
19. X. Sun, J. Deng, S. Liu, T. Yan, B. Peng, W. Jia, Z. Mei, H. Su, L. Fang, L. Liu, Appl. Phys. A **122**, 864 (2016)

20. S. Liu, X. Sun, B. Peng, H. Su, Z. Mei, Y. Huang, J. Deng, C. Su, L. Fang, L. Liu, J. Electroceram. **37**, 137–144 (2016)
21. Y. Li, L. Fang, L. Liu, Y. Huang, C. Hu, Mater. Sci. Eng. B **177**, 673–677 (2012)
22. X. Liu, H. Fan, J. Shi, Q. Li, Sci. Rep. **5**, 12699 (2015)
23. G. Liu, H. Fan, J. Xu, Z. Liu, Y. Zhao, RSC Adv. **6**, 48708–48714 (2016)
24. Z. Tang, Y. Huang, K. Wu, J. Li, J. Eur. Ceram. Soc. **38**, 1569–1575 (2018)
25. Z. Kafi, A. Kompany, H. Arabi, A. Khorsand Zak, J. Alloy. Compd. **727**, 168–176 (2017)
26. L. Sun, R. Zhang, Z. Wang, E. Cao, Y. Zhang, L. Ju, J. Alloy. Compd. **663**, 345–350 (2016)
27. E. Swatsitang, T. Putjuso, J. Eur. Ceram. Soc. **38**, 4994–5001 (2018)
28. J. Jumpatam, B. Putasaeng, T. Yamwong, P. Thongbai, S. Maensiri, Mater. Res. Bull. **77**, 178–184 (2016)
29. J. Jumpatam, P. Thongbai, T. Yamwong, S. Maensiri, Ceram. Int. **41**, S498–S503 (2015)
30. P. Thongbai, B. Putasaeng, T. Yamwong, S. Maensiri, J. Alloy. Compd. **509**, 7416–7420 (2011)
31. J. Boonlakhorn, P. Kidkhunthod, N. Chanlek, P. Thongbai, J. Eur. Ceram. Soc. **38**, 137–143 (2018)
32. J. Boonlakhorn, P. Thongbai, Ceram. Int. **43**, 12736–12741 (2017)
33. K. Prompa, E. Swatsitang, T. Putjuso, Ceram. Int. **44**, 20739–20748 (2018)
34. E. Swatsitang, K. Prompa, T. Putjuso, J. Mater. Sci. Mater. Electron. **29**, 12639–12651 (2018)
35. W. Hao, P. Xu, M. Wang, S. Yang, W. Yupeng, H. Wu, L. Sun, E. Cao, Y. Zhang, J. Alloy. Compd. **740**, 1159–1164 (2018)
36. X. Ouyang, M. Habib, P. Cao, S. Wei, Z. Huang, W. Zhang, W. Gao, Ceram. Int. **41**, 13447–13454 (2015)
37. Y.-H. Lin, J. Cai, M. Li, C.-W. Nan, J. He, Appl. Phys. Lett. **88**, 172902 (2006)
38. K. Prompa, E. Swatsitang, C. Saiyasombat, T. Putjuso, Ceram. Int. **44**, 13267–13277 (2018)
39. M. Newville, J. Synchrotron. Radiat. **8**, 96–100 (2001)
40. B. Ravel, M. Newville, J. Synchrotron. Radiat. **12**, 537–541 (2005)
41. S. Jesurani, S. Kanagesan, M. Hashim, I. Ismail, J. Alloy. Compd. **551**, 456–462 (2013)
42. B. Zhang, Q. Zhao, A. Chang, H. Ye, S. Chen, Y. Wu, Ceram. Int. **40**, 11221–11227 (2014)
43. X. Huang, H. Zhang, M. Wei, Y. Lai, J. Li, J. Alloy. Compd. **708**, 1026–1032 (2017)
44. B. Zhang, Q. Zhao, A. Chang, Y. Wu, J. Alloy. Compd. **663**, 474–479 (2016)
45. W. Tuichai, S. Danwittayakul, N. Chanlek, P. Thongbai, S. Maensiri, J. Alloy. Compd. **703**, 139–147 (2017)
46. Z. Weng, C. Wu, Z. Xiong, Y. Feng, H. AminiRastabi, C. Song, H. Xue, J. Eur. Ceram. Soc. **37**, 4667–4672 (2017)
47. B. Guo, P. Liu, X. Cui, Y. Song, Ceram. Int. **44**, 12137–12143 (2018)
48. J. Boonlakhorn, P. Kidkhunthod, B. Putasaeng, T. Yamwong, P. Thongbai, S. Maensiri, J. Mater. Sci. Mater. Electron. **26**, 2329–2337 (2015)
49. P. Kum-onsa, P. Thongbai, B. Putasaeng, T. Yamwong, S. Maensiri, J. Eur. Ceram. Soc. **35**, 1441–1447 (2015)
50. J. Shi, H. Fan, X. Liu, Y. Ma, Q. Li, J. Alloy. Compd. **627**, 463–467 (2015)
51. J. Boonlakhorn, P. Kidkhunthod, B. Putasaeng, P. Thongbai, Ceram. Int. **43**, 2705–2711 (2017)
52. E. Jansen, W. Schäfer, G. Will, J. Appl. Crystallogr. **27**, 492–496 (1994)
53. M.A. Subramanian, D. Li, N. Duan, B.A. Reisner, A.W. Sleight, J. Solid State Chem. **151**, 323–325 (2000)
54. J. Jumpatam, B. Putasaeng, T. Yamwong, P. Thongbai, S. Maensiri, J. Eur. Ceram. Soc. **34**, 2941–2950 (2014)
55. J. Jumpatam, A. Mooltang, B. Putasaeng, P. Kidkhunthod, N. Chanlek, P. Thongbai, S. Maensiri, Ceram. Int. **42**, 16287–16295 (2016)
56. M. Li, A. Feteira, D.C. Sinclair, A.R. West, Appl. Phys. Lett. **88**, 232903 (2006)
57. W. Tuichai, N. Thongyong, S. Danwittayakul, N. Chanlek, P. Srepusharawoot, P. Thongbai, S. Maensiri, Mater. Des. **123**, 15–23 (2017)
58. A.J. Moulson, J.M. Herbert, *Electroceramics: Materials, Properties, Applications*, 2nd edn. (Wiley, New York, 2003), p. 310
59. J. Zhao, C. Zhang, C. Hu, K. Lu, J. Eur. Ceram. Soc. **37**, 3353–3359 (2017)
60. T. Li, D. Liu, H. Dai, H. Xiang, Z. Chen, H. He, Z. Chen, J. Alloy. Compd. **599**, 145–149 (2014)
61. L. Ramajo, R. Parra, J.A. Varela, M.M. Reboredo, M.A. Ramírez, M.S. Castro, J. Alloy. Compd. **497**, 349–353 (2010)
62. S.-Y. Chung, J.-H. Choi, J.-K. Choi, Appl. Phys. Lett. **91**, 091912 (2007)
63. L.J. Liu, L. Fang, Y.M. Huang, Y.H. Li, D.P. Shi, S.Y. Zheng, S.S. Wu, C.Z. Hu, J. Appl. Phys. **110**, 094101 (2011)
64. Y. Huang, L. Liu, D. Shi, S. Wu, S. Zheng, L. Fang, C. Hu, B. Elouadi, Ceram. Int. **39**, 6063–6068 (2013)
65. Y. Huang, D. Shi, Y. Li, G. Li, Q. Wang, L. Liu, L. Fang, J. Mater. Sci. Mater. Electron. **24**, 1994–1999 (2013)
66. L. Liu, Y. Huang, Y. Li, D. Shi, S. Zheng, S. Wu, L. Fang, C. Hu, J. Mater. Sci. **47**, 2294–2299 (2012)
67. G. Li, Z. Chen, X. Sun, L. Liu, L. Fang, B. Elouadi, Mater. Res. Bull. **65**, 260–265 (2015)
68. W. Somphan, P. Thongbai, T. Yamwong, S. Maensiri, Mater. Res. Bull. **48**, 4087–4092 (2013)